



NONTRIVIAL POWER-LAW SCALING OF PEAK FORCES DURING GRANULAR IMPACT

Title	NONTRIVIAL POWER-LAW SCALING OF PEAK FORCES DURING GRANULAR IMPACT
Item Type	Thesis
Authors	Krizou, Nasser
URI	https://hdl.handle.net/10945/62766
Publisher	Monterey, CA; Naval Postgraduate School
Date Issued	2019-06
Rights	Copyright is reserved by the copyright owner.
Download date	2026-04-15 00:23:33
Link to Item	https://hdl.handle.net/10945/62766

Downloaded from NPS Archive: Calhoun



**NAVAL
POSTGRADUATE
SCHOOL**

MONTEREY, CALIFORNIA

THESIS

**NONTRIVIAL POWER-LAW SCALING OF PEAK
FORCES DURING GRANULAR IMPACT**

by

Nasser Krizou

June 2019

Thesis Advisor:
Second Reader:

Abram H. Clark IV
Christopher G. Smithro

Approved for public release. Distribution is unlimited.

THIS PAGE INTENTIONALLY LEFT BLANK

REPORT DOCUMENTATION PAGE			<i>Form Approved OMB No. 0704-0188</i>	
Public reporting burden for this collection of information is estimated to average 1 hour per response, including the time for reviewing instruction, searching existing data sources, gathering and maintaining the data needed, and completing and reviewing the collection of information. Send comments regarding this burden estimate or any other aspect of this collection of information, including suggestions for reducing this burden, to Washington headquarters Services, Directorate for Information Operations and Reports, 1215 Jefferson Davis Highway, Suite 1204, Arlington, VA 22202-4302, and to the Office of Management and Budget, Paperwork Reduction Project (0704-0188) Washington, DC 20503.				
1. AGENCY USE ONLY <i>(Leave blank)</i>		2. REPORT DATE June 2019	3. REPORT TYPE AND DATES COVERED Master's thesis	
4. TITLE AND SUBTITLE NONTRIVIAL POWER-LAW SCALING OF PEAK FORCES DURING GRANULAR IMPACT			5. FUNDING NUMBERS	
6. AUTHOR(S) Nasser Krizou				
7. PERFORMING ORGANIZATION NAME(S) AND ADDRESS(ES) Naval Postgraduate School Monterey, CA 93943-5000			8. PERFORMING ORGANIZATION REPORT NUMBER	
9. SPONSORING / MONITORING AGENCY NAME(S) AND ADDRESS(ES) N/A			10. SPONSORING / MONITORING AGENCY REPORT NUMBER	
11. SUPPLEMENTARY NOTES The views expressed in this thesis are those of the author and do not reflect the official policy or position of the Department of Defense or the U.S. Government.				
12a. DISTRIBUTION / AVAILABILITY STATEMENT Approved for public release. Distribution is unlimited.			12b. DISTRIBUTION CODE A	
13. ABSTRACT (maximum 200 words) Ballistic impact into a soil target has broad military relevance. Understanding the forces during impact is crucial to predicting damage and survivability. This process involves several nonlinear physical mechanisms, making it difficult to describe. While some existing models of ballistic impact characterize the average response during penetration well, these models fail during the initial stages of impact when forces are the largest. There currently is no theoretical framework for understanding the forces and dynamics during these crucial early stages. In this thesis, we use numerical simulations of intruders impacting granular media, coupled with existing experimental data, to understand the forces during the initial stages of impact. For slow impacts, forces are independent of speed and set by the weight of the intruder. For fast impacts, the impact forces grow as a non-linear power law in the impact velocity with exponent 4/3. This scaling depends on the size of the intruder and stiffness of the grains, and it is insensitive to gravity, friction, the nonlinear force law between grains, and the density of the intruder. We use dimensional analysis to collapse all data onto a single curve, providing a first step toward a comprehensive theoretical description of this process.				
14. SUBJECT TERMS granular material, intruder impact, ballistic impact, intruder-material interaction, numerical simulations, intruders impacting disks, microscopic intruder-grains interactions, early stages of impact, macroscopic ballistic models, nontrivial power law scaling, peak forces, initial transient phase, impact into granular materials, friction, nonlinear grain-scale force relation			15. NUMBER OF PAGES 61	
			16. PRICE CODE	
17. SECURITY CLASSIFICATION OF REPORT Unclassified	18. SECURITY CLASSIFICATION OF THIS PAGE Unclassified	19. SECURITY CLASSIFICATION OF ABSTRACT Unclassified	20. LIMITATION OF ABSTRACT UU	

THIS PAGE INTENTIONALLY LEFT BLANK

Approved for public release. Distribution is unlimited.

**NONTRIVIAL POWER-LAW SCALING OF PEAK FORCES DURING
GRANULAR IMPACT**

Nasser Krizou
Major, Canadian Army
BCE, Royal Military College of Canada, 2003

Submitted in partial fulfillment of the
requirements for the degree of

MASTER OF SCIENCE IN APPLIED PHYSICS

from the

**NAVAL POSTGRADUATE SCHOOL
June 2019**

Approved by: Abram H. Clark IV
Advisor

Christopher G. Smithro
Second Reader

Kevin B. Smith
Chair, Department of Physics

THIS PAGE INTENTIONALLY LEFT BLANK

ABSTRACT

Ballistic impact into a soil target has broad military relevance. Understanding the forces during impact is crucial to predicting damage and survivability. This process involves several nonlinear physical mechanisms, making it difficult to describe. While some existing models of ballistic impact characterize the average response during penetration well, these models fail during the initial stages of impact when forces are the largest. There currently is no theoretical framework for understanding the forces and dynamics during these crucial early stages.

In this thesis, we use numerical simulations of intruders impacting granular media, coupled with existing experimental data, to understand the forces during the initial stages of impact. For slow impacts, forces are independent of speed and set by the weight of the intruder. For fast impacts, the impact forces grow as a non-linear power law in the impact velocity with exponent $4/3$. This scaling depends on the size of the intruder and stiffness of the grains, and it is insensitive to gravity, friction, the nonlinear force law between grains, and the density of the intruder. We use dimensional analysis to collapse all data onto a single curve, providing a first step toward a comprehensive theoretical description of this process.

THIS PAGE INTENTIONALLY LEFT BLANK

TABLE OF CONTENTS

I.	INTRODUCTION.....	1
II.	BACKGROUND	3
III.	EXPERIMENTS AND SIMULATIONS SET-UP.....	11
	A. EXPERIMENTAL TECHNIQUES	11
	B. DEM SIMULATIONS.....	13
IV.	RESULTS	21
	A. EXPERIMENTAL DATA.....	22
	B. SIMULATION RESULTS	23
	1. Grain-Grain Interactions	25
	2. Intruder and Grains Parameters.....	27
	3. Spatial Dimensions.....	31
	4. Cluster of Grains Parameters	33
V.	ANALYSIS	35
	A. PEAK FORCE	35
	B. TIME AT PEAK FORCE	36
	C. NUMERICAL SOLUTION TO THE ADDED MASS MODEL.....	37
VI.	CONCLUSIONS	43
	LIST OF REFERENCES	45
	INITIAL DISTRIBUTION LIST	47

THIS PAGE INTENTIONALLY LEFT BLANK

LIST OF FIGURES

Figure 1.	Representation of the three stages of an impact into a granular material. Source: [2].....	3
Figure 2.	Dynamics of an intruder during impact into a granular material. (a) Depth of the intruder as a function of time, (b) Velocity of the intruder, in the y-component (vertical), as a function of time. Source: [2].....	4
Figure 3.	Comparison between a macroscopic force law, Poncelet model (black dashed line), recorded force acting on an intruder during impact (blue), time averaged recorded force acting on an intruder during impact (red). Source: [5].....	5
Figure 4.	Fit of the drag coefficient ηz using experimental data. Blue circles represent the circular intruders (blunt), red triangles represent ogive intruders of ratio $a/b = 3$ (pointy) and green triangles represent ogive intruders of aspect ratio $a/b = 1$ (blunt). Source: [4].....	6
Figure 5.	(a) Acoustic activity in a photoelastic granular material associated to (c) the granular force response affecting an intruder during impact, over time. The force response is approximated as the sum of the discrete gradient squared, G^2t , of the (b) depth variation of the image intensity as a function of time. Source: [6].	7
Figure 6.	Geometry of interaction between grains	8
Figure 7.	Peak force and time at peak force as a function of intruder initial velocity for experiments of an intruder impacting into a dense suspension. Source: [9].	9
Figure 8.	Added mass model as depicted by Waitukaitis [9].....	10
Figure 9.	Bronze intruder impacting into a 2D photoelastic granular material. Experimental device built by Clark to investigate the microscopic grain-grain interactions controlling the forces affecting the intruder throughout its trajectory. The intruder is dropped from various heights translating into specific intruder impact velocities. Adapted from [6], [8].	12
Figure 10.	Sequential images of an intruder impacting into a 2D photoelastic granular material. Source: [6].	13

Figure 11.	Example image of a simulation of an intruder impacting a 2D granular material. Red gradient represents an increased pressure.	14
Figure 12.	Two particles colliding using a damped spring model	15
Figure 13.	Two particles shearing using a Cundall-Strack model	15
Figure 14.	Verification of a particle colliding with every particle in a system.....	17
Figure 15.	Object-oriented structure of the simulation code.....	18
Figure 16.	Verification of a particle colliding with its immediate neighbors	19
Figure 17.	Dynamic of an intruder during its course in a granular material. Simulation data. Dimensionless unit.....	21
Figure 18.	Peak force and time of occurrence as a function of intruder initial velocity. Experimental data	23
Figure 19.	Peak force and time of occurrence as a function of intruder initial velocity. Simulation data. Dimensionless units.	24
Figure 20.	Peak force as a function of intruder weight for velocities below non-linear regime	25
Figure 21.	Peak force and time at peak force as a function of intruder initial velocity. Hertzian (smaller icons) vs linear interactions. Dimensionless units.	26
Figure 22.	Peak force and time at peak force as a function of intruder initial velocity. Frictional vs frictionless interactions. Dimensionless units.....	27
Figure 23.	Peak force and time at peak force as a function of intruder initial velocity. Intruder density and size. Dimensionless units.....	28
Figure 24.	Peak force as a function of intruder density.....	29
Figure 25.	Peak force and time at peak force as a function of intruder initial velocity. Grain stiffness. Dimensionless units.....	30
Figure 26.	Peak force and time at peak force as a function of intruder initial velocity. Gravity. Dimensionless units.	31
Figure 27.	Peak force and time at peak force as a function of intruder initial velocity. 3D simulations. Dimensionless units.	32
Figure 28.	Example of a grain cluster influenced by the intruder. Color indicates a normalized magnitude of the particle's velocity pointing	

along a specific axis. Red indicates a negative velocity in the z component, green is a positive velocity in the z component and blue is the absolute value of the x component. The junction between white grains and colored grain represent the force front propagating outwards33

Figure 29. Non-linear scaling of the cluster’s mass, M_c , and the average speed, v_{avg} , in the vertical component of all grains in that cluster as a function of the intruder’s initial velocity34

Figure 30. Dimensionless solution for the magnitude of the peak force.....36

Figure 31. Dimensionless solution for the time at peak force.....37

Figure 32. Peak force and time at peak force comparison between impact into dense suspension (vibrant colored dots) and dry granular material. η is the viscosity of the liquid and ϕ is the packing fraction of the granular material38

Figure 33. Dynamic of an intruder impacting in a dense suspension. numerical solution for an intruder of density 6400 kgm^3 39

Figure 34. Peak acceleration and time at peak force of an intruder impacting in a dense suspension. Numerical solution based on intruder’s speed.....40

Figure 35. Peak acceleration and time at peak force of an intruder impacting in a dense suspension. (a) and (b) are from numerical solution based on bulk sound speed of the material, (c) and (d) are based on intruder’s speed and bulk sound speed of the material.....41

Figure 36. Adjusted added mass model.....42

THIS PAGE INTENTIONALLY LEFT BLANK

I. INTRODUCTION

This thesis attempts to further the understanding of ballistic impact into granular materials by studying the peak force affecting an intruder in the early stages of penetration into a granular material. This study includes the analysis of unpublished experimental data obtained from a previous research as well as results from extensive discrete element method (DEM) simulations. In the present study, we analyze the peak force and time at which peak force occurs as a function of intruder size and density, grain stiffness, normal and tangential force interaction models, gravity, and spatial dimension of the system. This thesis is organized into six chapters:

1. Chapter I Introduction
2. Chapter II Background
3. Chapter III Experimental and Simulations Set-up
4. Chapter IV Results
5. Chapter V Analysis
6. Chapter VI Conclusions

Chapter II provides a brief overview of past studies on intruder penetration in granular material along with a discussion on limitation of current models used to describe the dynamics between grains and intruder. Chapter III describes the experiments, conducted during previous research, and the DEM simulations from which the data analyzed in this study were obtained. Chapter IV and V present and analyze the experimental data and simulation results. Conclusions and recommendations for follow-on work are given in Chapter VI.

THIS PAGE INTENTIONALLY LEFT BLANK

II. BACKGROUND

The physics of impact into a granular material is a ubiquitous phenomenon of great significance. Applications include the more obvious asteroid impact and missile defense as well as the less obvious, but more commonplace locomotion on sand and dirt. Although we do not fully understand the physical properties of granular materials, we have learned how to use the most common granular material to build resilient and self-healing defenses against projectiles (trenches, sandbags, Hesco bastion) and to give them careful considerations when planning amphibious operations and land operations. The relevance of granular impact in so many aspects of our lives has made it a popular subject of study for several decades [1]. Additionally, recent technological advances, such as high-speed cameras and high-performance computing, have made it possible to study the problem from a grain-scale perspective.

Enabled by these advances, Pica Ciamarra recorded and tracked the motions of an intruder, depicted in Figure 1, as well as conducted simulation of impacts into granular material using the discrete element method (DEM) [2]. He showed that an intruder's impact into a granular material can be broken down into three separate stages (impact, penetration, and collapse). Figure 1 depicts the intruder's progression through the granular material in each of those three stages.

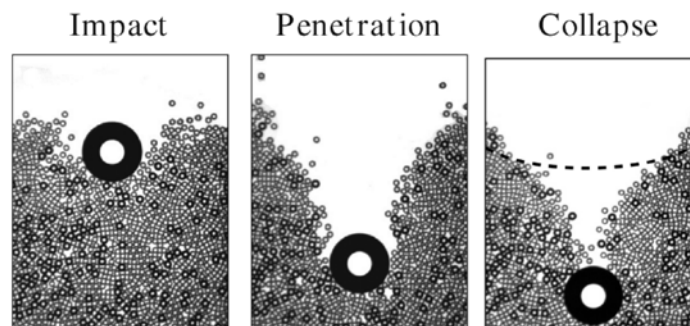


Figure 1. Representation of the three stages of an impact into a granular material. Source: [2].

Figure 2 depicts the motion dynamics of the intruder throughout the event, with each stage, separated by dashed lines, harboring different dynamic behaviors. During the impact stage, the projectile rapidly decelerates, and during the penetration stage, the mean acceleration is constant. During the collapse stage, the projectile has almost stopped and the particles above it are collapsing to fill the gap created by the penetration [2]. To better understand what characterizes the force on the intruder during the impact phase—when the time-averaged, macroscopic force law models fail to capture the forces affecting the intruder—this thesis will specifically focus on classifying what sets the peak forces at impact.

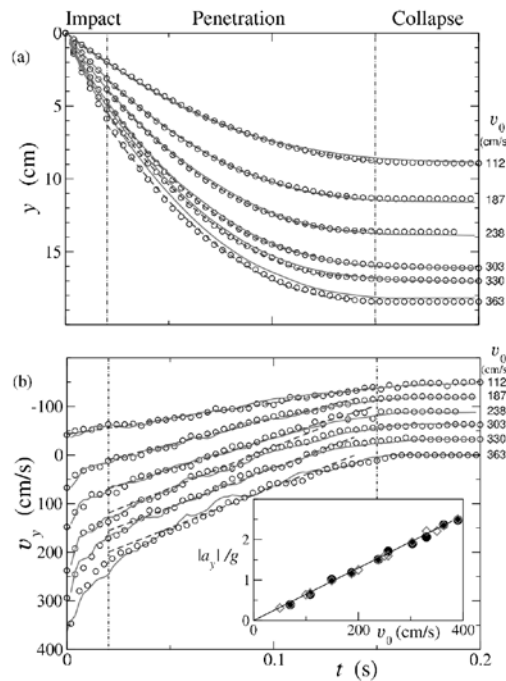


Figure 2. Dynamics of an intruder during impact into a granular material. (a) Depth of the intruder as a function of time, (b) Velocity of the intruder, in the y -component (vertical), as a function of time. Source: [2].

The long and sustained scientific interest in this field gave rise to several models able to approximate the dynamics between an intruder and granular material during impact. Without a practical way to look at the microscopic grain-grain interactions these models are usually conceived using space-time averaged macroscopic force laws and assumptions

of relevant physical principles to derive the various terms in its law [3], [4]. The most common model, often called the Poncelet model, is valid during the penetration phase of the impact process. It can be generalized by the following depth-dependent equation:

$$m_i \ddot{z}_i = m_i g - f(z_i) - h(z_i) \dot{z}_i^2 \quad (1)$$

Here, z_i and m_i , represent the depth and mass of the intruder, g is gravity, and dots denote time derivatives. The functions $f(z_i)$ and $h(z_i) \dot{z}_i^2$ are depth-dependent terms that account for the yielding of the material and inertial drag from the material, respectively. Figure 3 shows how the Poncelet model, Equation (1), captures the time-averaged motion of the intruder during the impact. However, we see that rapid fluctuations in time are not entirely captured by this model. These fluctuations are particularly large at the moment of impact, in agreement with Figure 2.

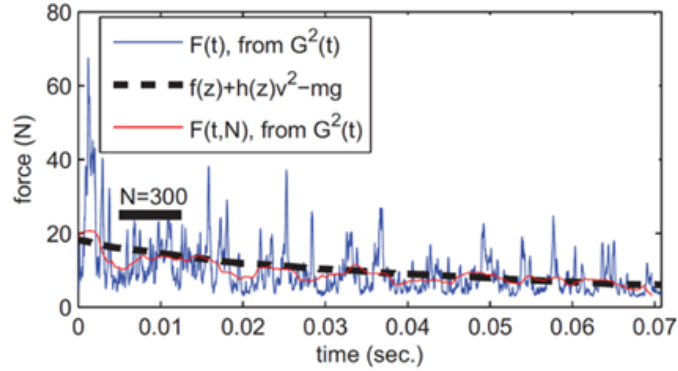


Figure 3. Comparison between a macroscopic force law, Poncelet model (black dashed line), recorded force acting on an intruder during impact (blue), time averaged recorded force acting on an intruder during impact (red). Source: [5].

Figure 4 depicts a large collection of impact data, involving intruders of various sizes, shapes and aspect ratios, fitted to the Poncelet model, Equation (1) [4]. This figure shows that the drag coefficient, $h(z_i)$, is relatively constant at mid-course, is well described by the Poncelet model during the penetration phase. However, at the initial stage, called the impact phase in Figure 1, $h(z_i)$ fluctuates significantly and the Poncelet model diverges

from experimental results. We see that $h(z_i)$ is higher for more blunt intruders and lower for pointy intruders. These forces during the very early stages of impact represent the largest forces that will be experienced during the entire process, and thus they are most important for fracture, survivability, and other failure-related measures. Understanding the forces right at the initial stages of impact (including how discrepancies away from a constant drag coefficient arise from interactions at the grain scale) is the subject of this thesis.

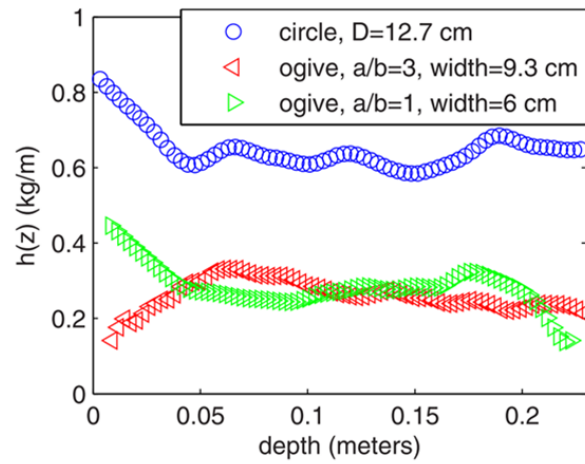


Figure 4. Fit of the drag coefficient $h(z)$ using experimental data. Blue circles represent the circular intruders (blunt), red triangles represent ogive intruders of ratio $a/b = 3$ (pointy) and green triangles represent ogive intruders of aspect ratio $a/b = 1$ (blunt). Source: [4].

Capturing images of intruders impacting into 2D beds of photoelastic disks using a highspeed camera, Clark was able to see the force interaction at the microscopic level [4], [5], [6], [7], [8]. The association between the acoustic activity below the intruder's edge and the magnitude of the forces affecting its course, shown in Figure 5, emphasize that the forces in the granular material, which generate the forces back on the intruder, are strongly dependent on how force is transmitted from one grain to the next along complex networks known as force chains. Clark showed the acoustic activity present at the leading edge of the intruder controls the intruder's motion and the large force fluctuations at short time scale [6].

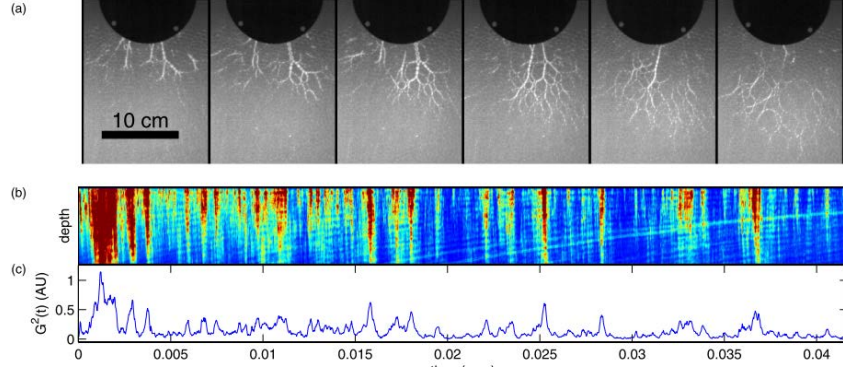


Figure 5. (a) Acoustic activity in a photoelastic granular material associated to (c) the granular force response affecting an intruder during impact, over time. The force response is approximated as the sum of the discrete gradient squared, $G^2(t)$, of the (b) depth variation of the image intensity as a function of time. Source: [6].

At the initial moments of impact, there is a shock that propagates away from the intruder. The speed at which this shock propagates follows a nonlinear power-law that depends on the details of the nonlinear interactions between grains and the initial velocity of the intruder [8]. These relationships are described by the following equations.

$$\frac{v_f}{v_b} \propto \left(\frac{v_0}{v_b}\right)^{\frac{\alpha-1}{\alpha+1}} \quad (2)$$

$$f = E^* w d \left(\frac{\delta}{d}\right)^\alpha \quad (3)$$

Here, v_f is the force propagation speed, v_b is a characteristic sound speed inside a grain, v_0 is the speed of the intruder right at impact, E^* , d and w are the effective Young's modulus, diameter and thickness of a grain, δ is the displacement, and $\alpha \approx 1.4$ for the disk-shaped photoelastic grains used in these studies. The geometry of the grain interaction is depicted in Figure 6.

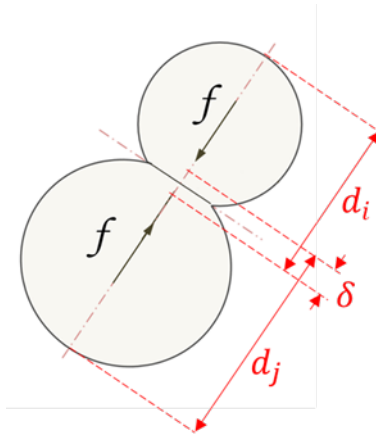


Figure 6. Geometry of interaction between grains

Assuming system boundaries are sufficiently far away, the peak force affecting the intruder during impact is limited to a finite number of grains reached by the forces as they propagate through the granular medium. Thus, a reasonable assumption might be that the nonlinear force law described by Equation (3), which sets the speed and spatial structure of shock propagation, might also control the magnitude and time scale of the peak force during the early stages of the impact. Thus, varying the grain scale properties in Equations. (2) and (3) (e.g., E^* , d , α , v_b) would provide a convenient way to test this hypothesis, which we do in this thesis.

Finally, we note the results from a parallel field of study regarding impacts into dense suspensions, where grains are suspended in a Newtonian fluid such as water. Waitukaitis and Jaeger [9] investigated impact-activated solidification of dense suspensions showing plots of peak force on an intruder and its time of occurrence as a function of intruder's initial velocity. Interestingly, their results (depicted in Figure 7) shows how both relationships follow power law relations with approximate slopes $4/3$ (for peak acceleration) and $-2/3$ (for time of peak acceleration). As we will show in this thesis, these slopes are similar to the case we study here, namely intruders impacting into dry granular materials [10]. The apparent agreement between these two cases suggests that this power law scaling maybe a universal property for impact into particulate materials.

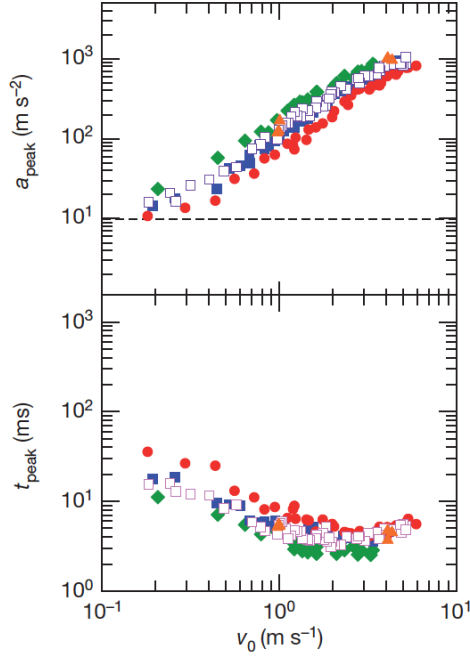


Figure 7. Peak force and time at peak force as a function of intruder initial velocity for experiments of an intruder impacting into a dense suspension. Source: [9].

Waitukaitis [9] suggested the intruder motion in a dense suspension can be solved numerically using an added mass model. The model describes the impact between the intruder and the dense suspension as an inelastic collision with a mass growing below the intruder as it penetrates the suspension, Figure 8. The growing mass causes an upward force against the intruder. The rod dynamics are captured by a force balance equation

$$(m_i + m_a) a_i = - \left(\frac{dm_a}{dt} \right) v_i + F_{ext}, \quad (4)$$

where F_{ext} comes from gravity, $F_g = -m_i g$, and the buoyant force of the suspension, $F_b \approx 1/3 \pi \rho g (r_i + k |z_i|)^2 |z_i|$. a_i, v_i, z_i are the acceleration, velocity and position of the intruder along a vertical axis. The growing mass, m_a is approximated as a mass with a cone-like volume that grows proportionally with the velocity of the intruder $m_a = c \rho g \frac{1}{3} \pi (R_i + K |z_i|)^2 |z_i|$. R_i is the radius of the intruder and $c = 0.37$ and $K = 12.5$ are empirical propagation constants.

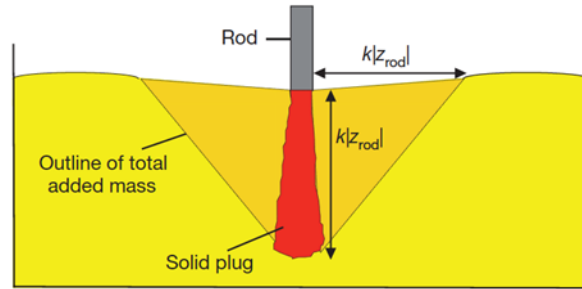


Figure 8. Added mass model as depicted by Waitukaitis [9]

III. EXPERIMENTS AND SIMULATIONS SET-UP

This thesis uses experiments and numerical simulations to study impact into granular materials. The experiments, involving intruders impacting 2D beds of photoelastic disks, were conducted by Clark in the context of research on nonlinear force propagation during granular impact [8]. This earlier paper studied only the force propagation speed and spatial structure. Here, we reuse the results of the same experiments, but focus instead on the intruder trajectories, from which we can extract the force on the intruder as a function of time. We also use custom DEM simulations to isolate key parameters and study their effects on the peak force affecting the intruder and the time of its occurrence.

A. EXPERIMENTAL TECHNIQUES

These experiments were carried out using the protocol described in Refs. [6] and [8]. Since these experiments were conducted by a different team, for a different research goal, the techniques used will not be described in detail. In summary, the experiments dropped thin circular metal intruders into 10,000 thin photoelastic disks sandwiched between two thick Plexiglass sheets, as shown in Figure 9. The density of the intruder was varied using bronze and aluminum as its composition material, its size varied between diameters of 6.35 cm, 10.16 cm, 12.7 cm and 20.32 cm, and its speed varied between $0.0 \leq v_0 \leq 6.6$ m/s. The stiffness of the photoelastic disks was varied by using three different photoelastic materials, cut into disks of size 0.6 cm and 0.9 cm.



Figure 9. Bronze intruder impacting into a 2D photoelastic granular material. Experimental device built by Clark to investigate the microscopic grain-grain interactions controlling the forces affecting the intruder throughout its trajectory. The intruder is dropped from various heights translating into specific intruder impact velocities. Adapted from [6], [8].

The motion of the intruder and spatial structure of forces within the bed were captured using a high-speed camera; images of the results are shown in Figure 10. From these experiments we obtained the position, velocity, and acceleration of the intruder as a function of time, as well as the photoelastic signal from the grains, which is roughly proportional to the force. Through a review of the spatial structure of the forces we can confirm that at the time peak force is reached, the root like force networks did not reach the boundaries of the system. Since there was no influence from the boundaries, the force affecting the intruder at the time of peak force originate entirely from the granular material.

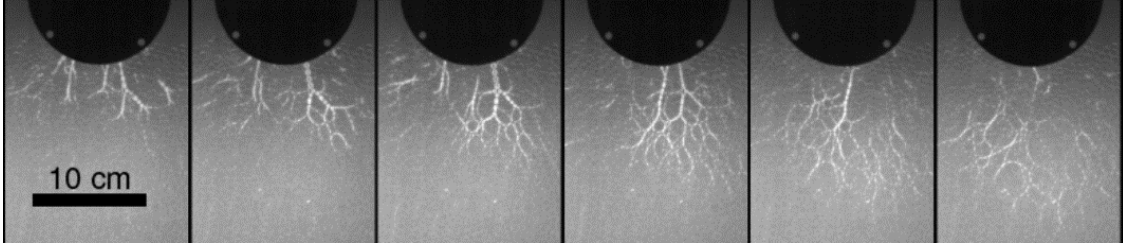


Figure 10. Sequential images of an intruder impacting into a 2D photoelastic granular material. Source: [6].

B. DEM SIMULATIONS

To compare with the results of these experiments, we ran simulations of intruders impacting into a granular material composed of 10,000 grains using the protocol described in Ref. [7]. An example from the simulation is shown in Figure 11. The simulations used dimensionless intruder and particle parameters similar to the experiments. To prevent the formation of ordered lattices in the bed we used equal numbers of large and small grains, with diameters d and $1.4d$, where the grain mass is proportional to its diameter squared. We added an element of randomness to the simulations by creating five randomly generated granular beds for each set of parameters simulated. Each granular bed used a different seed for our random number generator and the results shown in this paper are the ensemble averages of those simulations. The intruder diameter was varied between $5d$, $10d$ and $15d$, and its density was varied between 1 and 4 times the grain density. The velocity of the intruder at contact was varied over four orders of magnitude. Gravity was varied by a factor of 4. To study the influence of grain-grain interactions on the peak force affecting the intruder and the time of its occurrence we ran simulations with linear and nonlinear normal force interactions, as well as frictionless and frictional tangential force interactions using various grain stiffness. We also ran 2-dimensional and 3-dimensional simulations to study the effect of changing the spatial dimension.

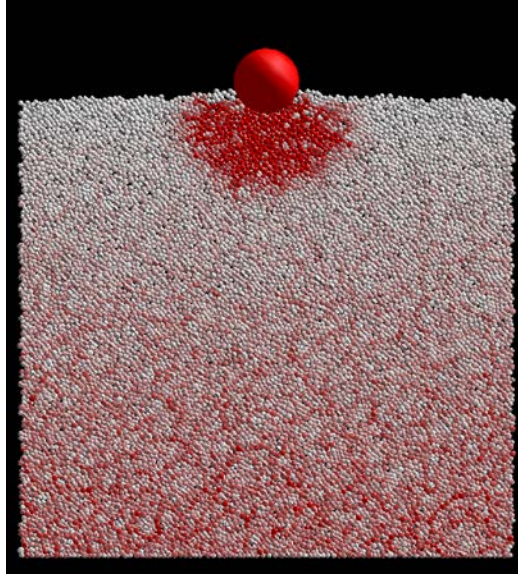


Figure 11. Example image of a simulation of an intruder impacting a 2D granular material. Red gradient represents an increased pressure.

The normal force interaction between the grain is computed using a damped spring force equation,

$$F_{i,j}^n = [k_n x^\alpha - \gamma_n m v_{i,j}]n, \quad (5)$$

where k_n is the spring stiffness constant related to the material property of the particles, x is the relative displacement between the particles, m is the reduced mass between particle i and j , $v_{i,j}$ is the relative velocity between particle i and j and n is the unitary vector pointing along the center-to-center distance between the two grains in contact. α is the Hertz coefficient. We set $\alpha = 1$ to simulate linear interactions between particles $\alpha = 3/2$ for nonlinear (Hertzian) interactions [11]. The damping term $\gamma_n m v_{i,j}$ removes energy during collisions, and it is related to the restitution coefficient e_n via $\gamma_n = -2 \frac{\ln e_n}{\tau_c}$. We set $e_n = 0.2$, and ignore any velocity dependence. Figure 12 depicts the normal force interactions between two particles colliding in this model.

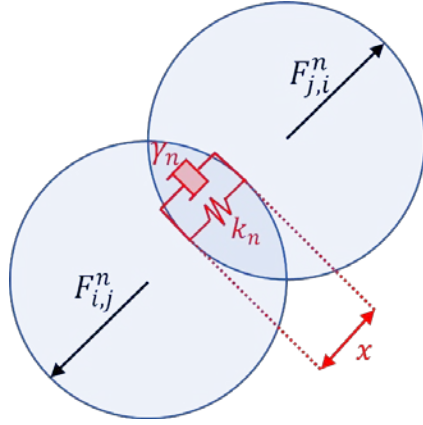


Figure 12. Two particles colliding using a damped spring model

When friction is enabled, the tangential force interaction between the grains is treated using a Cundall-Strack model [12]

$$F_{i,j}^t = -\text{sgn}(\xi_t) \min(k_t |\xi_t|, \mu F_{i,j}^n). \quad (6)$$

Here, $\xi_t = \int_{t_0}^t v_t dt$ is the elongation of an imaginary tangential spring with t_0 the time at which the particles touch each other and v_t the relative tangential velocity of the contact point between two grains. k_t is the stiffness of the tangential spring and μ is the coefficient of friction. For our simulations, we set $\mu = 0.3$ and $k_t = k_n/3$. Figure 13 depicts the tangential force interaction between two particles in this model.

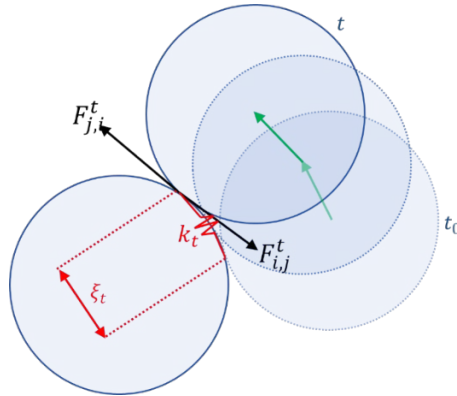


Figure 13. Two particles shearing using a Cundall-Strack model

The simulations use Newton's second law of motion to resolve the forces applied on the intruder and on each grain at every timestep,

$$m_i \frac{d^2 r_i}{dt^2} = F_{i,j}^n + F_{i,j}^t + m_i g \quad (7)$$

Rotational motion is described by

$$I_i \frac{d\omega_i}{dt} = -\frac{1}{2} d_i n \times F_{i,j}^t, \quad (8)$$

where r_i, I_i, ω_i, d_i are the position, moment of inertia, angular velocity and diameter of the intruder, respectively.

The velocity and position of every particle is obtained by integrating the equations of motion with a velocity Verlet algorithm [13].

$$r_i(t + \Delta t) = r_i(t) + v_i(t)\Delta t + \frac{1}{2} a_i(t) \Delta t^2 \quad (9)$$

$$v_i(t + \Delta t) = v_i(t) + \frac{1}{2} (a_i(t) + a_i(t + \Delta t)) \Delta t \quad (10)$$

In this case, a velocity Verlet integration provides a good approximation without sacrificing too much performance when compared to other popular integration algorithms (Euler, Runge Kutta).

The system has wrapped periodic boundaries along the horizontal axis and solid boundaries along the vertical axis. Although our simulation uses relatively simple equations, it must verify whether or not every particle in the system collides with every another at each timestep. This process cannot be vectorized and must be repeated for every particle in the system. Figure 14 demonstrates how particle 1 is compared with particles 2, 3, 4 and 5 to evaluate the forces affecting its trajectory. Since the distance between the centers of particles 1 and 2 is shorter than the sum of their radius, particle 1 is in contact with particle 2. The distances between the center of particle 1 and the centers of particles 3, 4 and 5 are greater than the sum of their radius, therefore none of these particle touches particle 1.

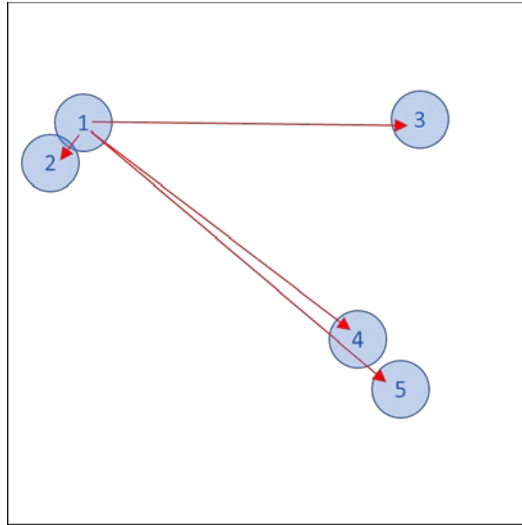


Figure 14. Verification of a particle colliding with every particle in a system

Using this contact detection algorithm, the performance of the simulation scales $O(N^2)$, where N is the number of particles in the system. To ensure the peak force is not influenced by forces reflected or transferred by the boundaries, we found a system of approximately 10,000 particles is necessary. We also ran simulations with less particles (1000, 2000, 4000) to confirm that system size did not influence our results. We are satisfied this is the case; however, the peak force affecting the intruders with higher initial kinetic energy were heavily influenced by the boundaries. To properly analyze all the possible parameters affecting the peak force (gravity, particle stiffness, intruder velocity, intruder size, intruder density, grain-grain interactions, degrees of freedom) we require over 10,000 simulations, which would take weeks, if not months, on the cluster computer, using the current MATLAB code.

Three steps were taken to optimize the memory footprint and performance of the simulations. First, we converted the existing MATLAB code to C++, which runs significantly faster with a lower memory footprint. Second, we converted from procedural code to object-oriented code to improve its efficiency. Although the conversion to object-oriented does not automatically improve performance, treating particles as objects greatly simplifies the use of more abstract patterns, such as linked list, hash tables and sparse

matrices, which enables systemic enhancements to increase the overall efficiency. Figure 15 shows the overall structure of the object-oriented program. Conversion to object-oriented code also hides the underlying complexity of the DEM algorithms from the user, making the code easier to maintain and upgrade.

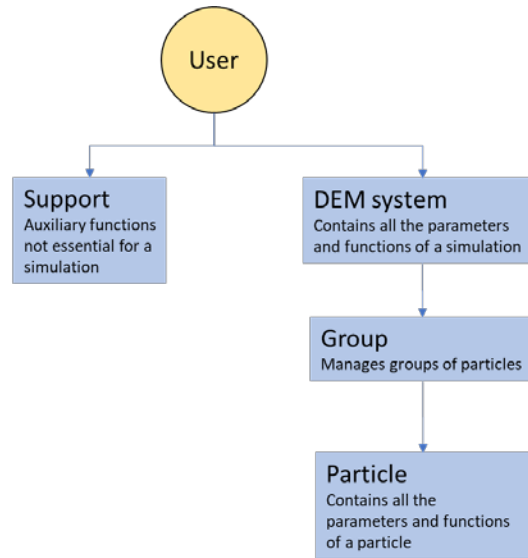


Figure 15. Object-oriented structure of the simulation code

Lastly, we improved the detection collision algorithm by limiting the number of particles being verified to those within a certain range. Figure 16 shows how this was achieved using a cell list algorithm [14] where each particle is assigned a cell based on its coordinates. Like our previous algorithm, the program iterates through every particle in the system; however, it only verifies if a collision occurs for particles contained in adjacent cells. Using a cell list contact detection algorithm, the performance of the simulation now scales as $O(N \log N)$, drastically improving performance for systems sized above 1000 particles.

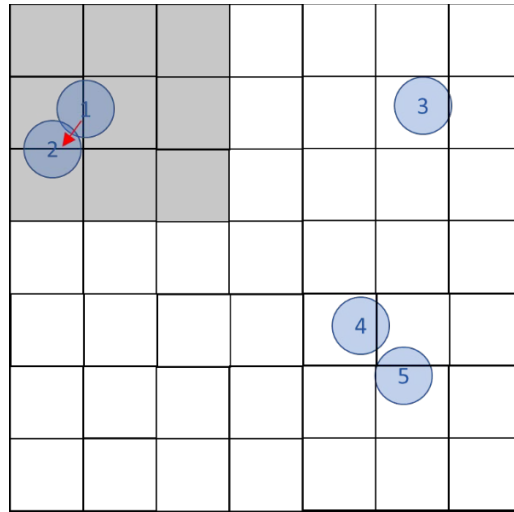


Figure 16. Verification of a particle colliding with its immediate neighbors

THIS PAGE INTENTIONALLY LEFT BLANK

IV. RESULTS

The raw data collected from the experiments and simulations consist of the forces affecting the intruder and the trajectory of the intruder as a function of time, including its velocity and position. Figure 17 shows the result obtained from a single DEM simulation of an intruder of diameter 15 and density 8 impacting into a granular material at velocity 12.8. The force from the granular bed acting on the intruder quickly climb to a peak and gradually decreases to a magnitude equivalent to the force of gravity acting on the intruder.

The object of this thesis is to understand the peak force exerted by the grains onto the intruder throughout the event. The second peak observed on the force curve is representative of a force being reflected by the bottom and sides boundaries of the bed. The system was scaled in size and the restitution coefficient tuned to prevent any ambiguity between the force originating from a direct impact into the grains and this reflected force. The results of more than 10,000 simulations were extracted and processed, using MATLAB, to capture the peak force, the time of its occurrence and the initial parameters of interest associated with that particular experiment or simulation (intruder diameter, density and velocity at impact, grain stiffness, friction coefficient, gravity constant, type of model used for grain-grain interaction, number of dimensions).

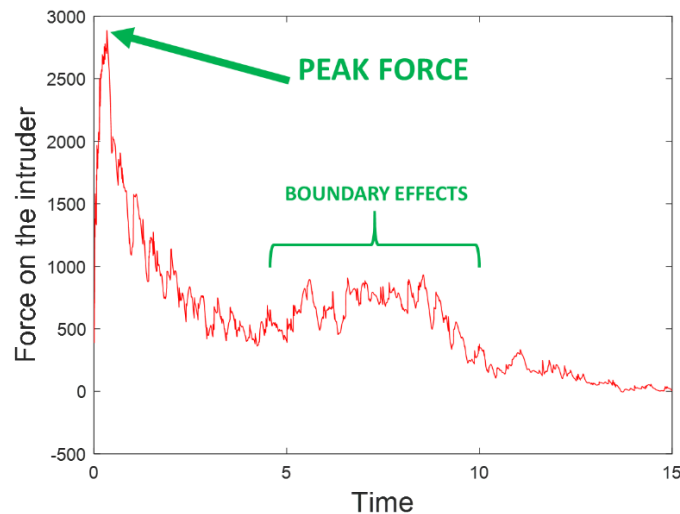


Figure 17. Dynamic of an intruder during its course in a granular material. Simulation data. Dimensionless unit

A. EXPERIMENTAL DATA

Using the experimental data, we plot the peak force over the range of intruder initial velocities. Panel (a) of Figure 18 shows the peak force experienced by the intruder as a function of its initial velocity for different intruder sizes; panel (b) of the figure shows the time of the peak force, also as a function of the initial velocity and for multiple shapes and sizes.

From the plateau, we see that for slow intruder speeds the magnitude of the peak forces exerted onto the intruder is independent of speed and is set by the weight of the intruder. The force of gravity on the intruder, by size, is 0.65N, 1.63N, 2.54N and 6.5N for the bronze intruder and 0.78N for the aluminum intruder. For fast intruder speeds, the peak forces grow as a non-linear power law scaling with the impact velocity $F_{max} \propto v_0^{4/3}$ in contrast with the Poncelet model which scales the force with $F \propto v_0^2$. Changes in intruder size and density result in quantitative offsets of the power law with the heavier intruders translating into an increase in the peak force. Variations in particle stiffness appears to have little to no effect on the magnitude of the peak force.

Panel (b) of Figure 18 shows that the time at peak force follows a power law $t_{max} \propto v_0^{-2/3}$ where the heavier intruders and softer particles take more time to reach peak force.

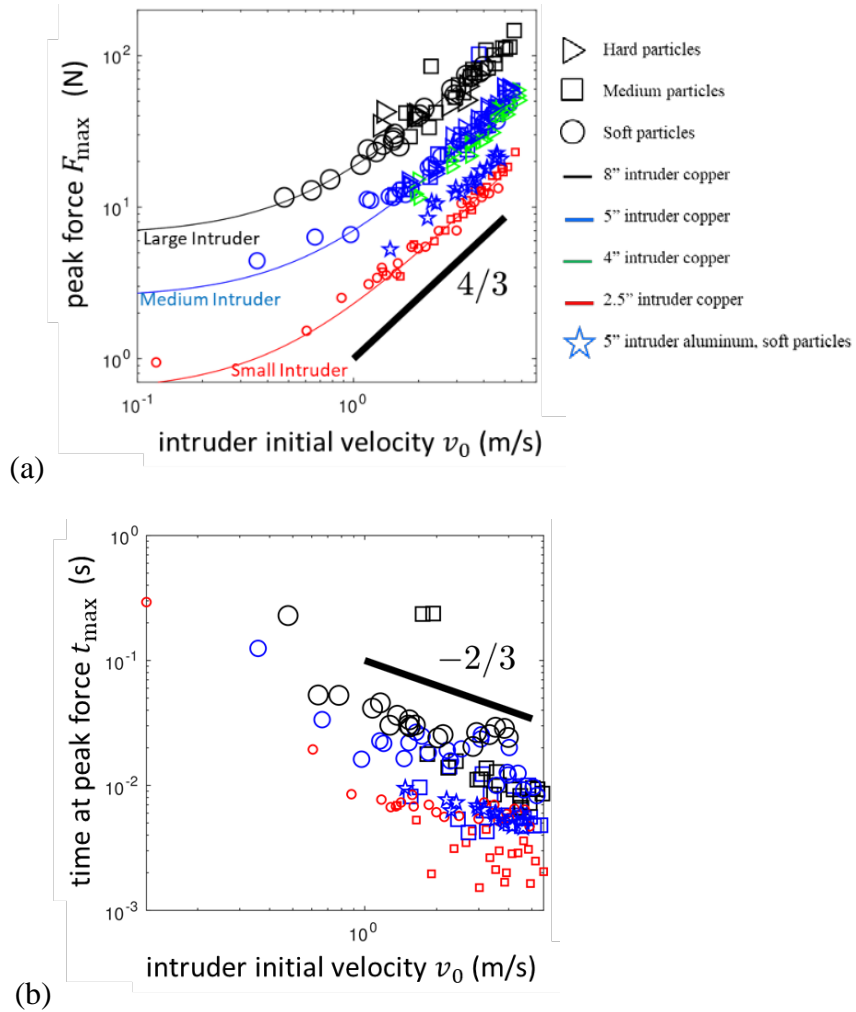


Figure 18. Peak force and time of occurrence as a function of intruder initial velocity. Experimental data

B. SIMULATION RESULTS

We used DEM simulations to isolate key parameters and demonstrate their effects on the magnitude and time of occurrence of the peak force. To assert the validity of our simulation we first compared the magnitude of the peak force obtained with the simulations with those from the experiments. The results of the simulations are shown in Figure 19 using the same format as the experimental results shown in Figure 18. From the figure we see the simulations provide curves that match closely the experiments on a logarithmic

scale, with the same non-linear scaling along $F_{max} \propto v_0^{4/3}$ and $t_{max} \propto v_0^{-2/3}$ as well as similar offsets due to intruder size.

More interestingly, this plot includes all variants of the grain-grain force laws used in our simulations (e.g., linear versus nonlinear springs, frictional versus nonfrictional interactions), and the strong agreement between live experiments and simulations is not limited to simulations with Hertzian frictional grain interactions. Simulations involving frictionless and linear grain interactions give essentially the same result. The extended range of intruder's initial velocities used for the simulations highlights the plateau obtained for F_{max} in the live experiments and unveil a change in the behavior of the t_{max} relation for lower speeds. At very slow intruder initial speed, t_{max} remains constant along a plateau strongly affected by the intruder's density and size.

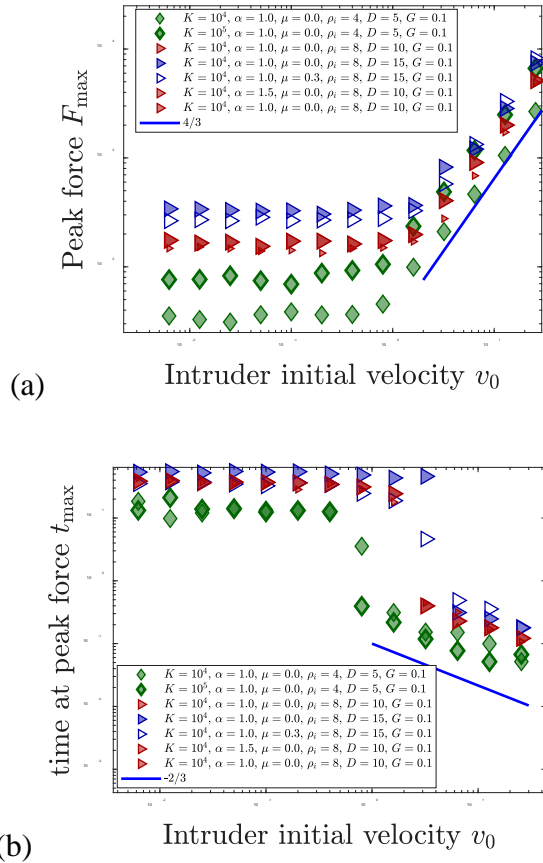


Figure 19. Peak force and time of occurrence as a function of intruder initial velocity. Simulation data. Dimensionless units.

We confirmed that for the plateau obtained in F_{max} and t_{max} the intruder is being accelerated by the force of gravity to a specific speed, beyond v_0 and highly dependent on its mass, before being slowed down to a stop by the material. Figure 20 shows how those plateau are highly dependent on the weight of the intruder. The mechanism that allow lighter, slow-moving intruders to reach higher peak force relative to their weight is unknown at this time.

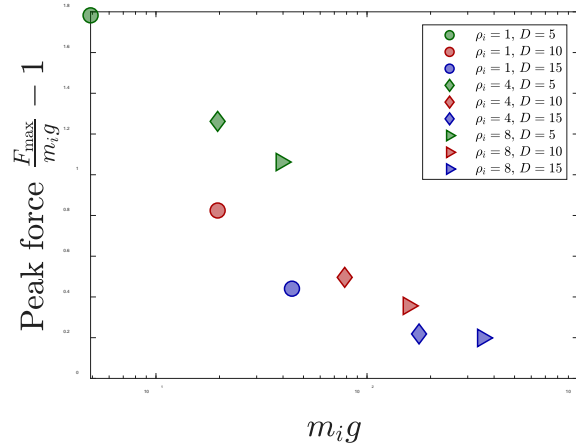


Figure 20. Peak force as a function of intruder weight for velocities below non-linear regime

1. Grain-Grain Interactions

To verify that Hertzian and linear interactions give the same result, we compare the peak force and its time of occurrence as a function of intruder's initial velocity between simulations with Hertzian interactions and simulations with linear interactions. Figure 21 illustrate how, although Hertzian interactions may have a slight impact on the shape of the power laws, it is insignificant compared to the phenomenon that scales the peak force along a slope of 4/3. The insensitivity to the type of interaction between grains depicted in the relation between t_{max} and v_0 reaffirm the fact that Hertzian interactions between grains is not what sets the peak forces.

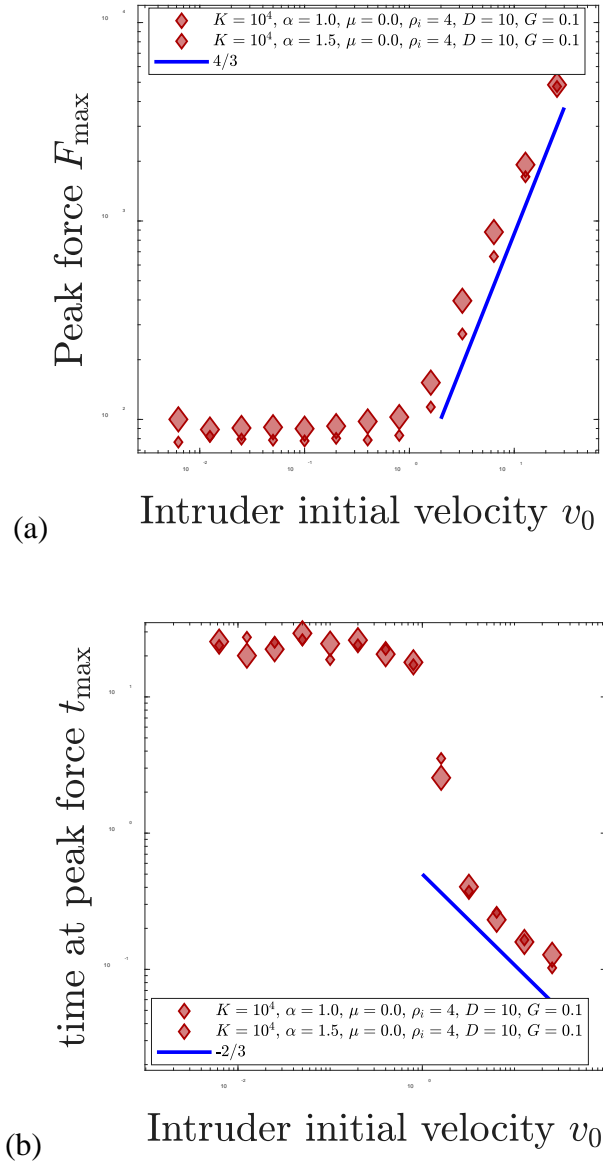
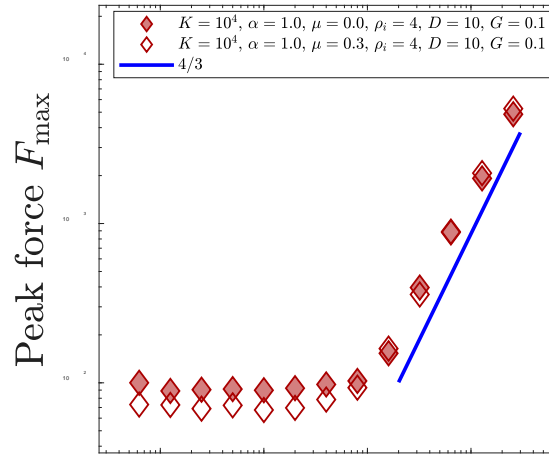
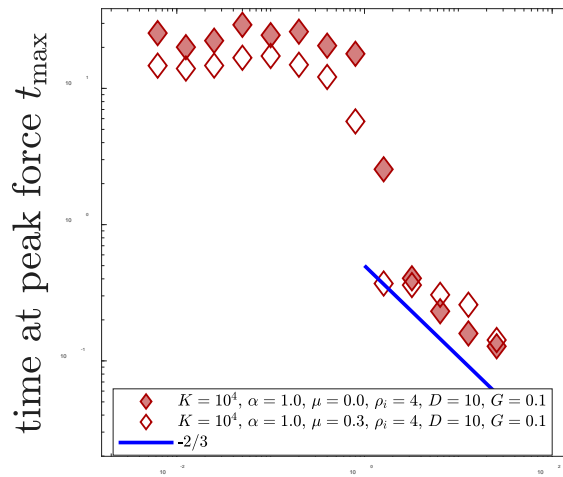


Figure 21. Peak force and time at peak force as a function of intruder initial velocity. Hertzian (smaller icons) vs linear interactions. Dimensionless units.

Next, we compare the peak force as a function of intruder's initial velocity between simulations with frictional and frictionless interactions. Figure 22 shows that, other than a slight offset, friction does not play a role in the magnitude of the peak force or the time of its occurrence.



(a) Intruder initial velocity v_0



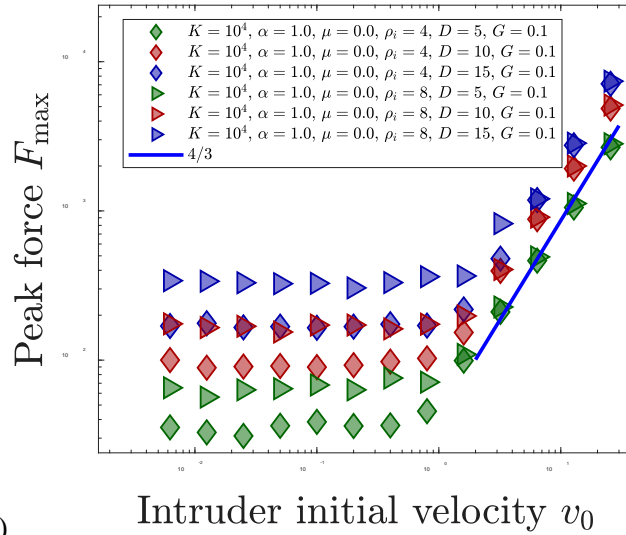
(b) Intruder initial velocity v_0

Figure 22. Peak force and time at peak force as a function of intruder initial velocity. Frictional vs frictionless interactions. Dimensionless units.

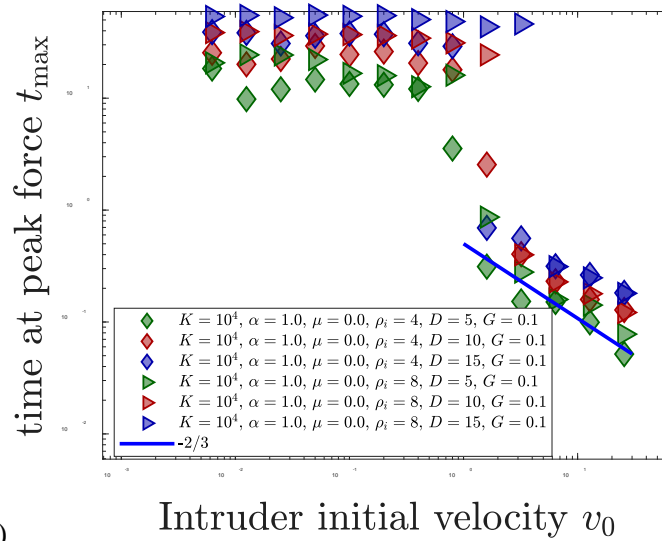
2. Intruder and Grains Parameters

Since Hertzian interactions and frictional interactions are not contributing to the peak force we compare the peak force for various intruder size and densities, using only frictionless linear interactions. Figure 23 shows that the contribution of the intruder density

to the peak force is insignificant, but the intruder's size does significantly offset the magnitude and time of occurrence of the peak force. Changes in size appear to scale the peak force linearly and does not appear to affect the $4/3$ slope of the peak force at higher speed. We also see that the $t_{\max}(v_0)$ relationship retain a slope of $-2/3$ for all intruder.



(a)



(b)

Figure 23. Peak force and time at peak force as a function of intruder initial velocity. Intruder density and size. Dimensionless units.

Figure 24 shows that the peak force appears to become independent of the value of intruder density for large densities.

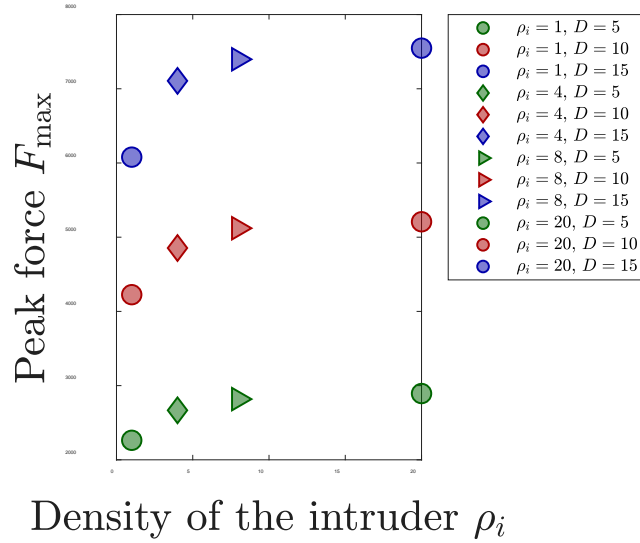


Figure 24. Peak force as a function of intruder density

Next we compare the peak force and its time of occurrence as a function of intruder's initial velocity while varying the grain's spring constant using linear interactions. According to Figure 25, the spring constant may play an important role in controlling the time of occurrence of the peak force and significantly offset the magnitude of the peak force. The fact that variations in grain stiffness result in a change in the $-2/3$ slope of the $t_{\max}(v_0)$ relationship suggesting that the relaxation time of the granular material may be an important component of the process leading to our peak force but does not entirely govern its magnitude.

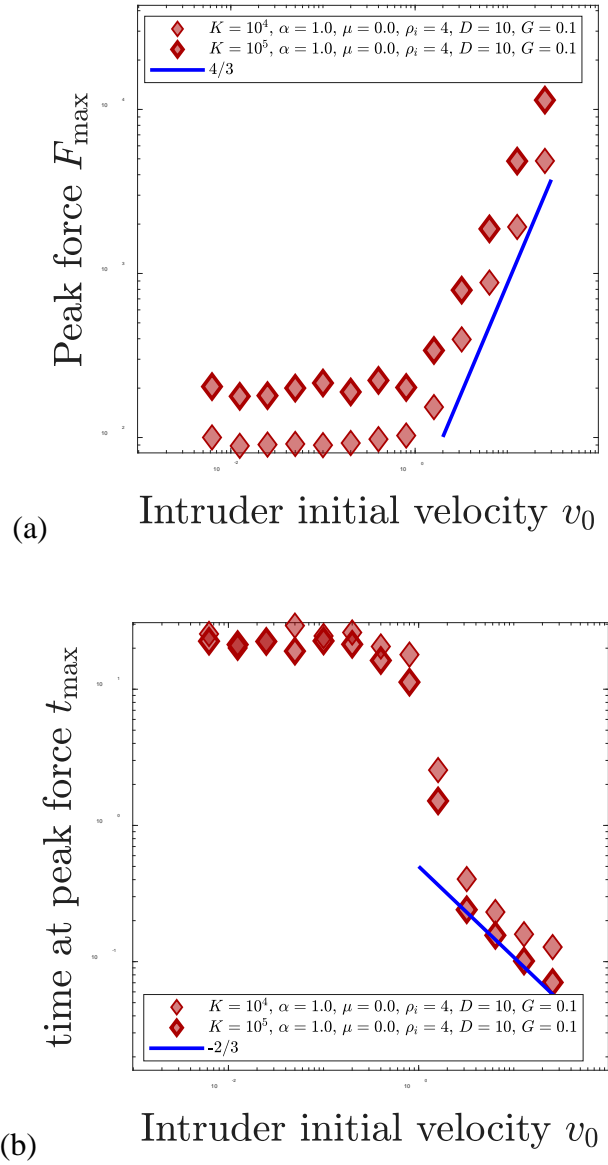


Figure 25. Peak force and time at peak force as a function of intruder initial velocity. Grain stiffness. Dimensionless units.

In Figure 26 we evaluate the effect of gravity over the same process. Gravity does not play a role at all at higher speeds. The fact that it does significantly affects the plateau in both relations adds to the validity that these plateau may be linked to the acceleration from gravity affecting the intruder as it slowly settles into the material at low impact speed.

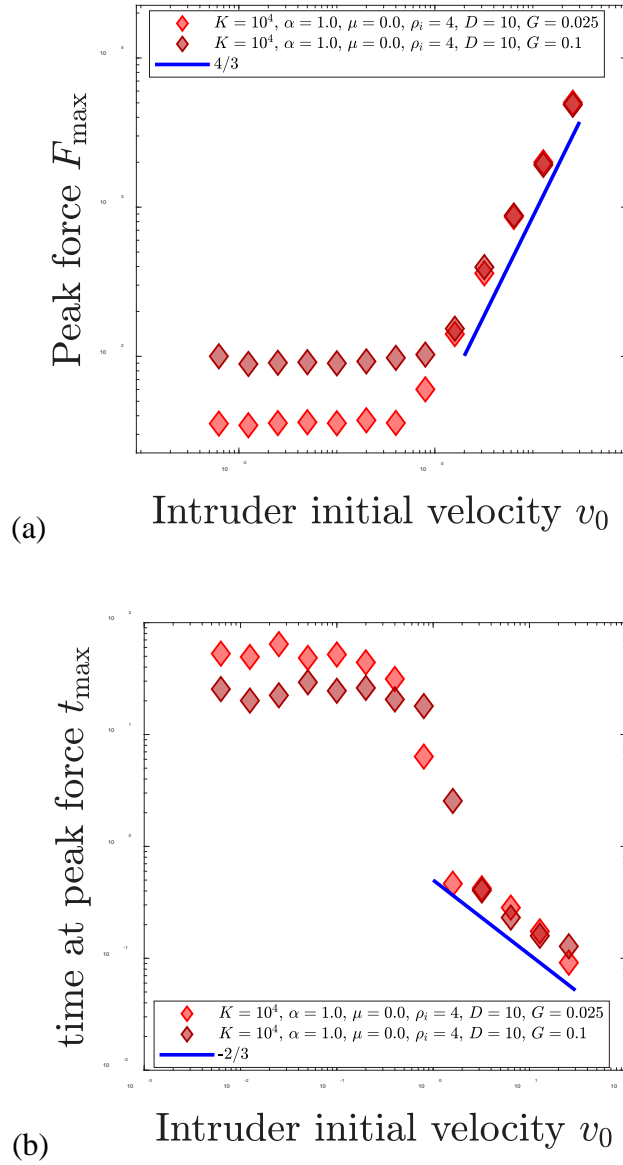


Figure 26. Peak force and time at peak force as a function of intruder initial velocity. Gravity. Dimensionless units.

3. Spatial Dimensions

Running 3D simulations with linear frictionless grain interactions, we looked at how adding an extra spatial dimension affects peak force and time at peak force. Figure 27 shows how the results obtained from the 3D simulations are also similar to results from the

experiments and the 2D simulations. We find plateau at low velocity that transitions to non-linear power laws of slope $4/3$, in the case of the peak force, and slope $-2/3$ for the time at peak force.

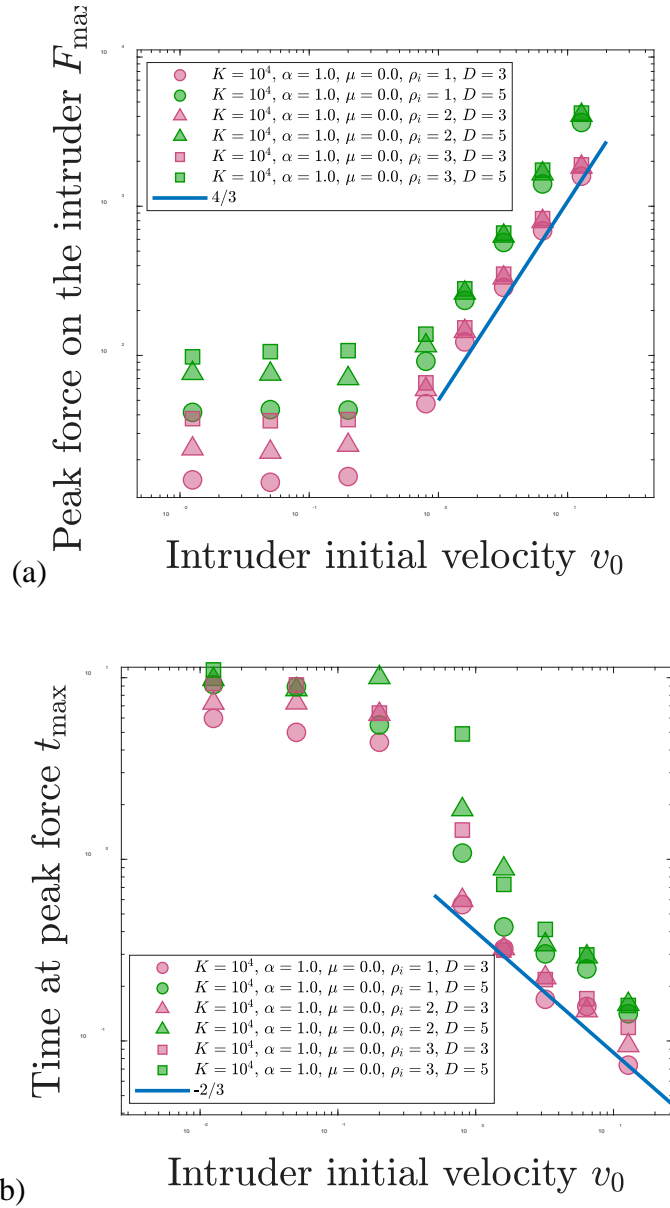


Figure 27. Peak force and time at peak force as a function of intruder initial velocity. 3D simulations. Dimensionless units.

4. Cluster of Grains Parameters

By selecting only grains that experienced a change in acceleration greater than 0.01% of their initial acceleration from the start of the simulation to the time at peak force we captured data on the cluster of grains influenced by the intruder. The data includes an extensive range of physical variables that are related to the systems parameter (i.e., potential energy, kinetic energy, momentum, average number of contacts between grain, mass, force, compression overlap, speed of the front, growth rate and distance traveled by the cluster).

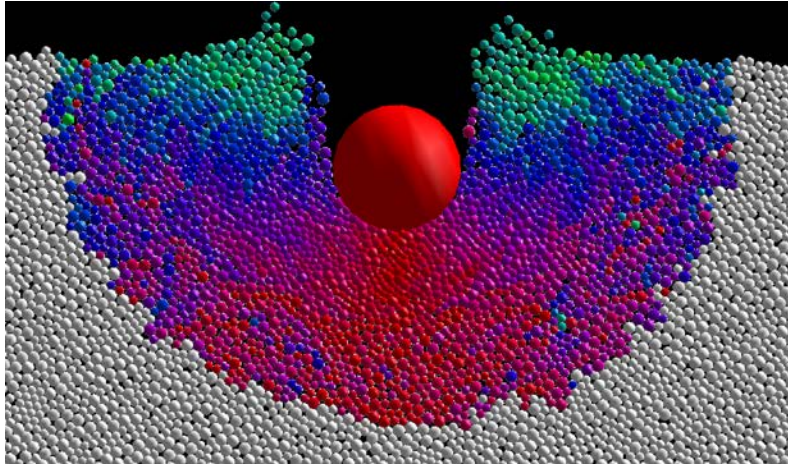


Figure 28. Example of a grain cluster influenced by the intruder. Color indicates a normalized magnitude of the particle's velocity pointing along a specific axis. Red indicates a negative velocity in the z component, green is a positive velocity in the z component and blue is the absolute value of the x component. The junction between white grains and colored grain represent the force front propagating outwards

Of the 53 variables tracked, three are worth mentioning as their scaling behavior follows non-linear power laws and could contribute to the non-linear scaling of F_{max} and t_{max} . The first variable, the total mass of the cluster, scales along $M_c \propto v_0^{-2/3}$ similar to the relation $t_{max}(v_0)$. The second variable the propagation radius of the force wave below the intruder scales along $z_{front} \propto v_0^{-1/3}$. This scaling is tied to the cluster mass as the

mass grows like a half circle with z_{front} representing its radius. The third variable, the average speed in the z component (vertical) of grains included in that cluster, scales along $v_{avg} \propto v_0^{4/3}$ similar to the relation $F_{max}(v_0)$. The scaling of the average speed of the grains contained in the mass suggest the peak force might be the result of how much mass is being accelerated at a given speed; therefore the added mass model proposed by Waitukaitis [9] could be contributing to the peak force of an impact into a granular material.

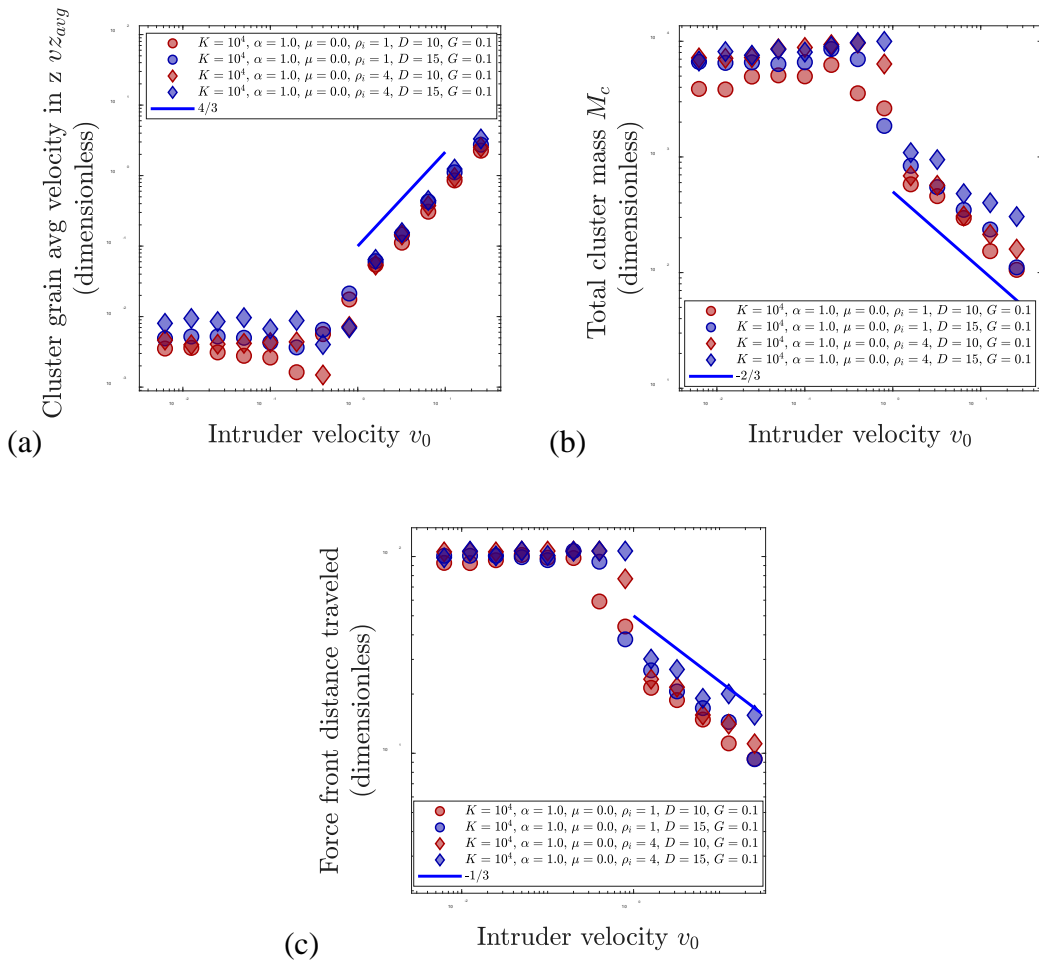


Figure 29. Non-linear scaling of the cluster's mass, M_c , and the average speed, v_{avg} , in the vertical component of all grains in that cluster as a function of the intruder's initial velocity

V. ANALYSIS

A. PEAK FORCE

We perform a dimensional analysis using Buckingham's Pi theorem [15] to obtain the relationship between the variables contributing to the peak force, F_{max} , and the time at peak force, t_{max} . The theorem states the solution to a problem involving n variables over k primary dimensions (e.g., time, length and mass) can be reduced to a physical equation involving a set of $n - k$ dimensionless parameters.

We showed that gravity, Hertzian interactions, friction, and number of spatial, dimensions had little to no effect on the magnitude of the peak force. We therefore assume for our dimensional analysis that the peak force is entirely determined by the diameter (D_g), density (ρ_g) and stiffness (K) of the grains, the diameter (D_i), density (ρ_i) and initial velocity (v_0) of the intruder. If our assumption is valid, we should find a solution to the magnitude of the peak force of the form

$$f(F_{max}, D_g, \rho_g, K, D_i, \rho_i, v_0) = 0. \quad (11)$$

Using Buckingham's Pi theorem, we subtract the 3 dimensions (time, length and mass) and obtain the following 4 dimensionless parameters, which Buckingham refers to as Pi groups,

$$\overline{F_{max}} = \frac{F_{max}}{D_g K}, \quad \overline{D_i} = \frac{D_i}{D_g}, \quad \overline{\rho_i} = \frac{\rho_i}{\rho_g} \quad \text{and} \quad \overline{v_0} = v_0 \sqrt{\frac{\rho_g}{K}}. \quad (12)$$

This gives us a dimensionless solution of the form

$$f\left(\frac{F_{max}}{D_g K}, \frac{D_i}{D_g}, \frac{\rho_i}{\rho_g}, v_0 \sqrt{\frac{\rho_g}{K}}\right) = 0 \rightarrow \frac{F_{max}}{D_g K} = f'\left(\frac{D_i}{D_g}, \frac{\rho_i}{\rho_g}, v_0 \sqrt{\frac{\rho_g}{K}}\right). \quad (13)$$

Experimenting with these parameters we obtain a satisfying collapse of our data scaling along a power law of slope 4/3 using the relation $\frac{\overline{F_{max}}}{\overline{D_i}}$ as a function of $\overline{v_0}$; this result is shown in Figure 30.

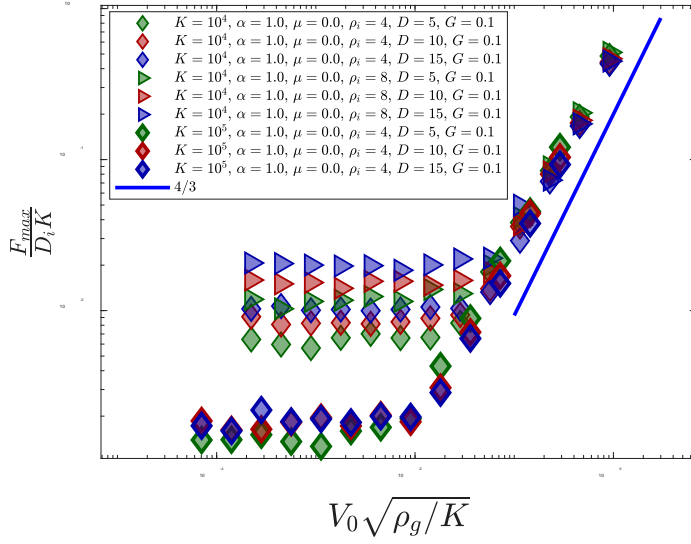


Figure 30. Dimensionless solution for the magnitude of the peak force

B. TIME AT PEAK FORCE

Going through the same exercise for t_{max} we should find a solution for the time at which peak force occurs of the form

$$f(t_{max}, D_g, \rho_g, K, D_i, \rho_i, v_0) = 0, \quad (14)$$

with the following 4 dimensionless parameters

$$\overline{t_{max}} = t_{max} \sqrt{\frac{K}{M_g}}, \quad \overline{D_i} = \frac{D_i}{D_g}, \quad \overline{\rho_i} = \frac{\rho_i}{\rho_g} \quad \text{and} \quad \overline{v_0} = v_0 \sqrt{\frac{\rho_g}{K}}, \quad (15)$$

to find a dimensionless solution of the form

$$f\left(t_{max} \sqrt{\frac{K}{M_g}}, \frac{D_i}{D_g}, \frac{\rho_i}{\rho_g}, v_0 \sqrt{\frac{\rho_g}{K}}\right) = 0 \rightarrow t_{max} \sqrt{\frac{K}{M_g}} = f'\left(\frac{D_i}{D_g}, \frac{\rho_i}{\rho_g}, v_0 \sqrt{\frac{\rho_g}{K}}\right). \quad (16)$$

Experimenting with these parameters we obtain a satisfying collapse of our data scaling along a power law of slope $-2/3$ using the relation $\frac{\overline{t_{max}}}{\overline{D_i}}$ as a function of $\overline{v_0}$; this result is shown in Figure 31.

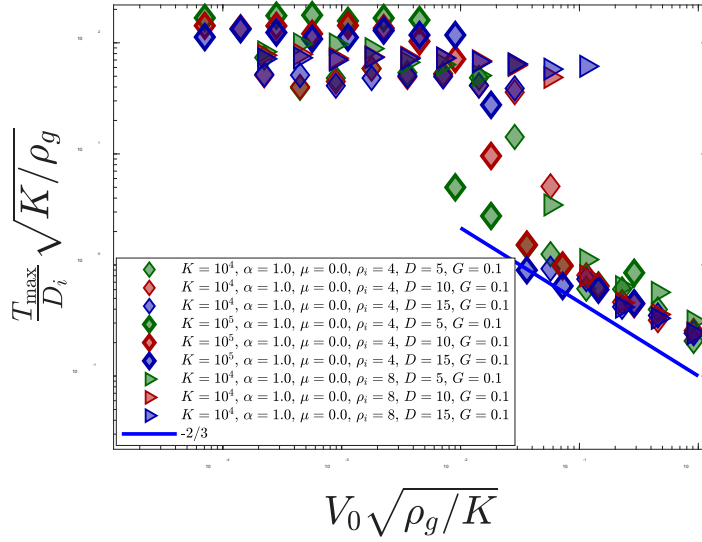


Figure 31. Dimensionless solution for the time at peak force

C. NUMERICAL SOLUTION TO THE ADDED MASS MODEL

Having determined the contribution of each parameter to the peak force and the time of the peak force, we find the non-linear scaling of $F_{max}(v_0)$ and $t_{max}(v_0)$ are not significantly affected by any parameters except the speed and physical size of the intruder as well as the stiffness and mass density of the grains. To get more insight on those non-linear scaling we turn to Waitukaitis' proposed added mass model that explains the process controlling the intruder's dynamics during an impact in a dense suspension [9]. Figure 32 shows how well the peak force he obtained from experiments matches the results from even the most basic 3D linear frictionless simulations.

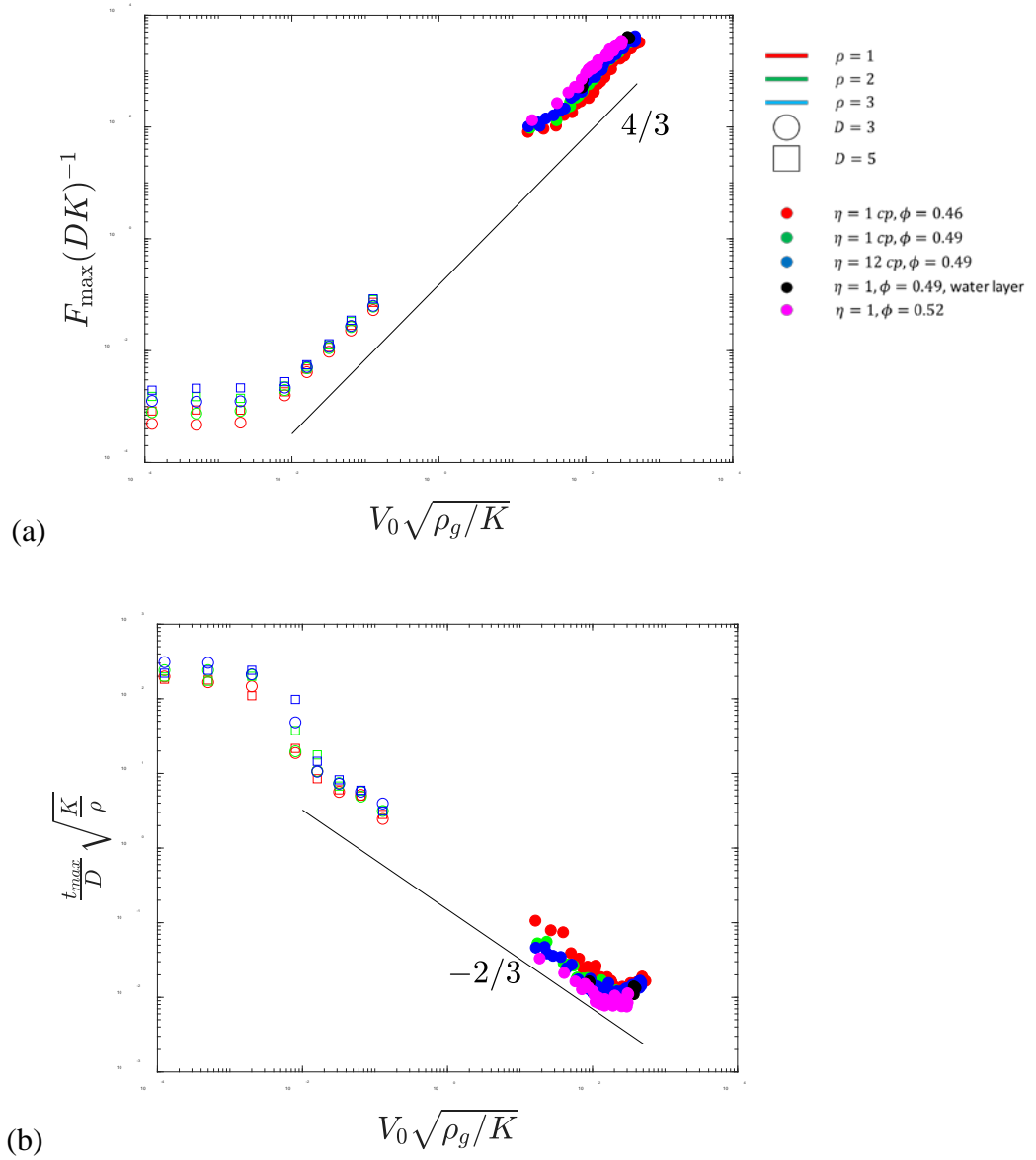


Figure 32. Peak force and time at peak force comparison between impact into dense suspension (vibrant colored dots) and dry granular material. η is the viscosity of the liquid and ϕ is the packing fraction of the granular material

We reproduced Waitukaitis’s numerical solution, described in the second chapter of this paper, to evaluate how his model applies to the peak force and the time at peak force for impacts into a granular material. Figure 33 shows the curves resulting from the

integration of equation (4) using MATLAB with the same solution parameters described in ref [9]. These curves show a behavior similar to the dynamics of an intruder impacting in a dry granular material displayed previously in Figure 2.

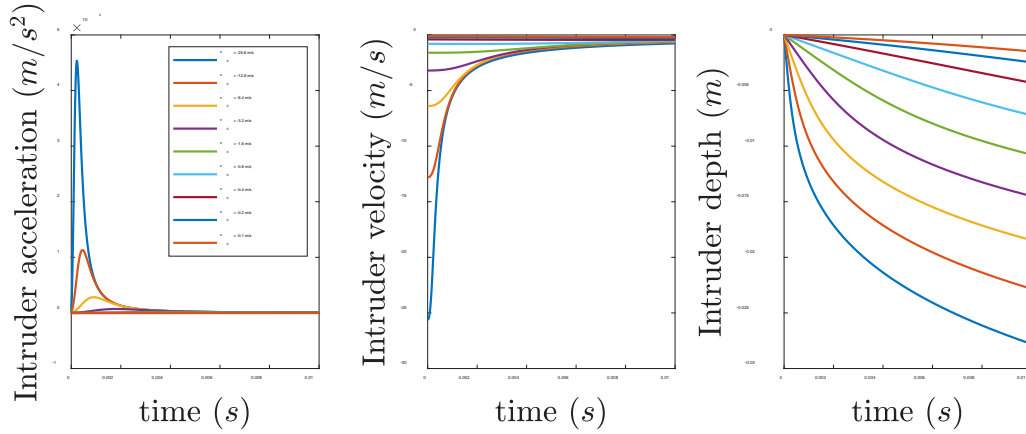


Figure 33. Dynamic of an intruder impacting in a dense suspension.
numerical solution for an intruder of density $6400 \frac{\text{kg}}{\text{m}^3}$

After extracting the peak acceleration and time at peak acceleration from the curves obtained, we analyzed their scaling along the initial velocity of the intruder. Figure 34 shows the peak acceleration of the intruder scaling along a power law of slope 2 and the time at peak acceleration scaling along a power law of slope -1. Although the dynamics of the intruder shown at Figure 33 do seem to match fairly well the overall dynamics of Waitukaitis live experiment, they do not agree with the peak acceleration he recorded at ref [9] and they do not agree with our scaling of $F_{max} \propto v_0^{4/3}$ and $t_{max} \propto v_0^{-2/3}$. The numerical solution also scales the peak acceleration linearly with the intruder's density, when experiments and simulations demonstrate that this scaling trends towards a plateau for high $\frac{\rho_i}{\rho_g}$ ratios.

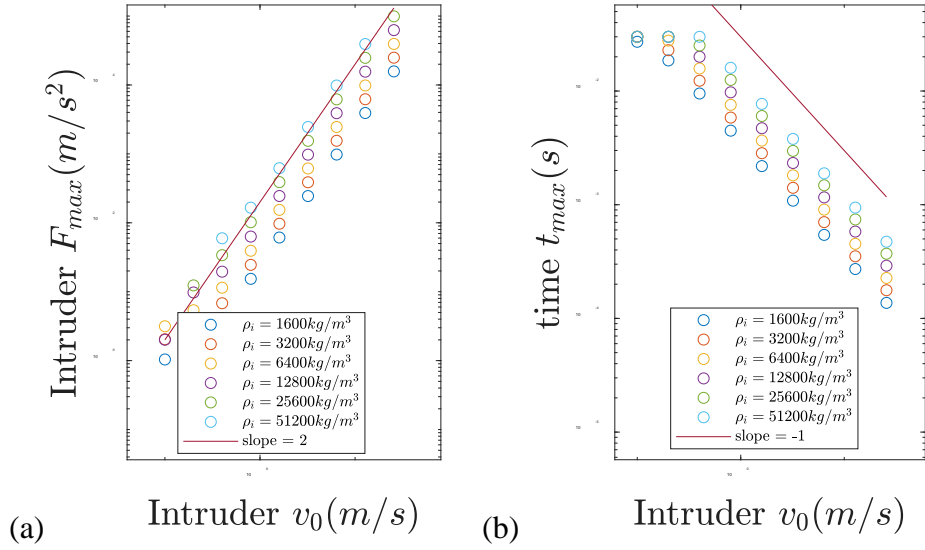


Figure 34. Peak acceleration and time at peak force of an intruder impacting in a dense suspension. Numerical solution based on intruder's speed.

Figure 35 shows results of Waitukaitis added mass numerical solutions modified to account for the geometry and speed of the force propagating in the material (z_{front}) when calculating the added mass. The panel (a) and (b) of the figure use a model where the propagation grows as a half sphere at a rate equivalent to the bulk sound speed in the material, $m_a = \rho_g \frac{1}{2} \frac{4}{3} \pi (v_b t)^3$. Since this model has the mass growing at a linear rate, F_{max} scales also linearly with the initial speed of the intruder, and t_{max} remains constant throughout. We saw earlier that $z_{front} \propto v_0^{1/3}$. Panel (c) of Figure 35 shows how, when we modify the added mass model to account for m_a dependence on v_0 , $m_a = \rho_g \frac{1}{2} \frac{4}{3} \pi \left(\left(\frac{v_0}{v_b} \right)^{1/3} v_b t \right)^3$, we obtain a scaling for F_{max} that agrees with our experiments and simulations $F_{max} \propto v_0^{4/3}$. Panel (d) shows, however, t_{max} scaling along $t_{max} \propto v_0^{-1/3}$. These results suggest that future work on the added mass model could result in an improved model able to capture more accurately the power law scaling we have demonstrated in this thesis. Figure 36 depicts a modified added mass model where the mass grows at a none linear rate after the intruder's impact with the granular material.

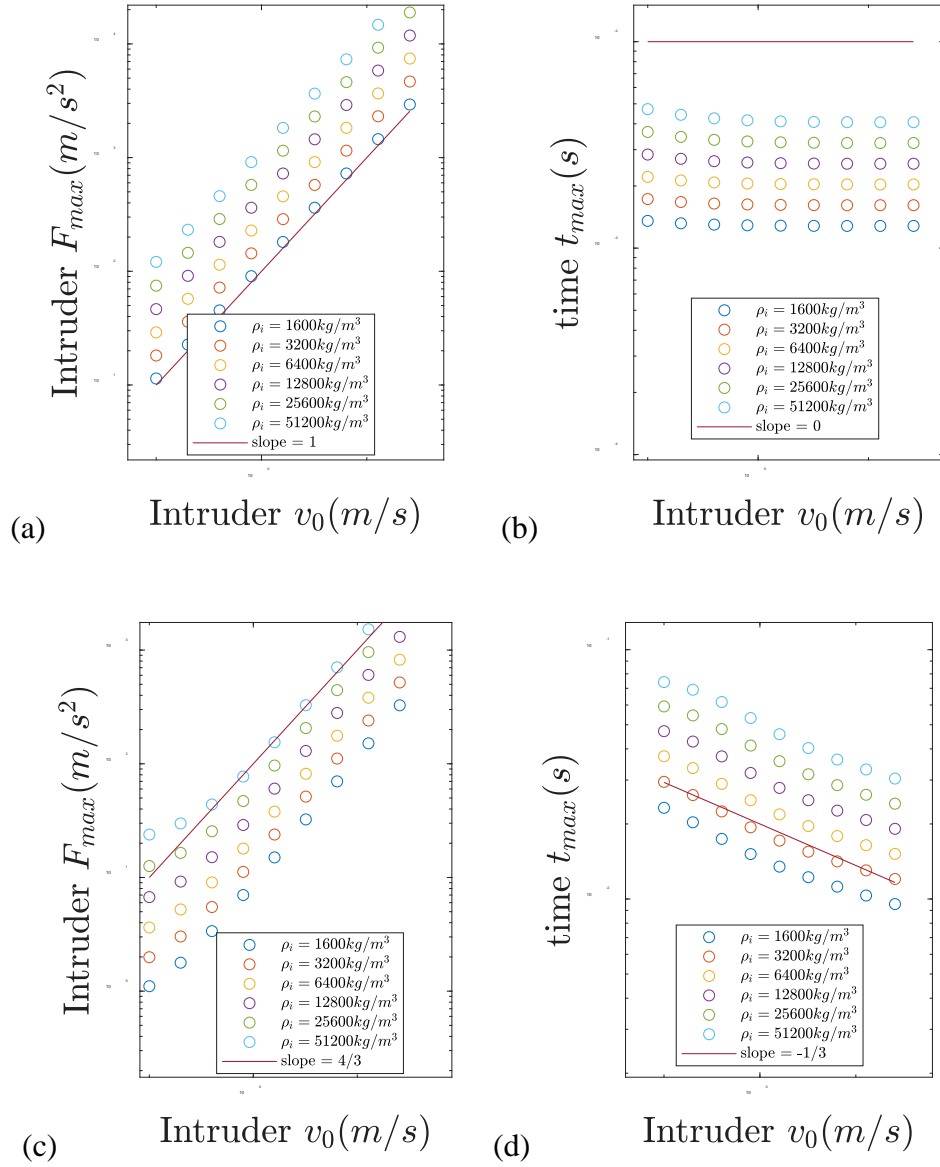


Figure 35. Peak acceleration and time at peak force of an intruder impacting in a dense suspension. (a) and (b) are from numerical solution based on bulk sound speed of the material, (c) and (d) are based on intruder's speed and bulk sound speed of the material

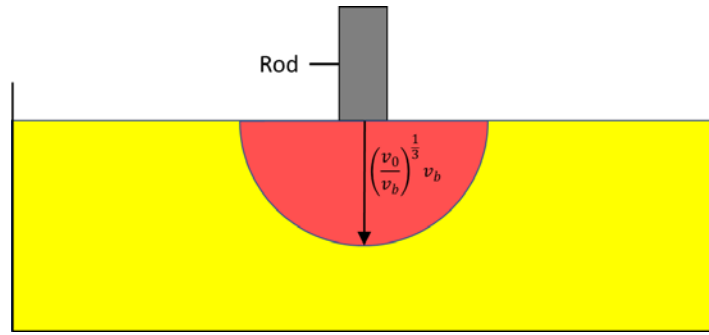


Figure 36. Adjusted added mass model

VI. CONCLUSIONS

The main objective of this thesis was to understand what characterize the forces during the initial stages of impact in a granular material. We accomplished our objective using experimental and DEM simulated data to classify what sets the peak forces at impact. We then performed a dimensional analysis to obtain the relationship between the variables contributing to the peak force, F_{max} , and the time at peak force, t_{max} .

For slow impacts, forces are independent of speed and are set by the weight of the intruder. For fast impacts, the peak forces grow as a non-linear power law in the impact velocity with exponent $4/3$ and the time at peak force scales as a non-linear power law in the impact velocity with exponent $-2/3$. These scaling depend qualitatively on the velocity of the intruder and they depend quantitatively on the size of the intruder and the relaxation time of the granular material $t_{relaxation} = \sqrt{\frac{m}{E^*}}$ [16], where m is the mass of a grain and E^* the effective Young's modulus of the granular material. F_{max} and t_{max} are insensitive to gravity, friction, the nonlinear force law between grains, and the density of the intruder.

We also showed that, in its current form, the numerical solution to the added mass model proposed by Waitukaitis [9] does not return the expected scaling behavior for the peak force and time at peak force. However, with future work, the numerical solution may be modified so that the added mass model more accurately capture the forces affecting the intruder during the early stage of impact.

THIS PAGE INTENTIONALLY LEFT BLANK

LIST OF REFERENCES

- [1] J. Duran, *Sands, Powders, and Grains: An Introduction to the Physics of Granular Materials*. Springer Science & Business Media, December 2012.
- [2] M. P. Ciamarra et al., “Dynamics of drag and force distributions for projectile impact in a granular medium,” *Phys. Rev. Lett.*, vol. 92, no. 19, p. 194301, May 2004.
- [3] W. A. Allen et al., “Dynamics of a Projectile Penetrating Sand,” *J. Appl. Phys.*, vol. 28, no. 3, pp. 370–376, March 1957.
- [4] A. H. Clark and R. P. Behringer, “Granular impact model as an energy-depth relation,” *Europhys. Lett.*, vol. 101, no. 6, p. 64001, March 2013.
- [5] A.H. Clark et al., “Collisional model for granular impact dynamics,” *Phys. Rev. E*, vol. 89, no. 1, p. 012201, Jan 2014.
- [6] A. H. Clark et al., “Particle Scale Dynamics in Granular Impact,” *Phys. Rev. Lett.*, vol. 109, no. 23, p. 238302, December 2012.
- [7] A. H. Clark et al., “Steady flow dynamics during granular impact,” *Phys. Rev. E*, vol. 93, no. 5, p. 050901, May 2016.
- [8] A. H. Clark et al., “Nonlinear Force Propagation During Granular Impact,” *Phys. Rev. Lett.*, vol. 114, no. 14, p. 144502, April 2015.
- [9] S. R. Waitukaitis and H. M. Jaeger, “Impact-activated solidification of dense suspensions via dynamic jamming fronts,” *Nature*, vol. 487, no. 7406, p. 205, July 2012.
- [10] A.H. Clark, “Peak force affecting intruder impacting granular material,” unpublished.
- [11] E. T. a. H. R. E. Dintwa, “On the accuracy of the Hertz model to describe the normal contact of soft elastic spheres,” *Granular Matter*, vol. 10, no. 3, pp. 209–221, March 2008.
- [12] P. A. Cundall and O. D. L. Strack, “A discrete numerical model for granular assemblies,” *Géotechnique*, vol. 29, no. 1, pp. 47–65, March 1979.

- [13] L. Verlet, “Computer Experiments on Classical Fluids,” *Phys. Rev.*, vol. 159, no. 1, p. 98, July 1967.
- [14] “Cell lists,” 02 April 2019. [Online]. Available: https://en.wikipedia.org/wiki/Cell_lists.
- [15] E. Buckingham, “On Physically Similar Systems; Illustrations of the Use of Dimensional Equations,” *Phys. Rev.*, vol. 4, no. 4, p. 345, October 1914.
- [16] C. Campbell, “Granular shear flows at the elastic limit,” *J Fluid Mech.*, vol. 465, pp. 261–291, August 2002.

INITIAL DISTRIBUTION LIST

1. Defense Technical Information Center
Ft. Belvoir, Virginia
2. Dudley Knox Library
Naval Postgraduate School
Monterey, California